

## Supporting Information

### **Broad Transparency and Wide Band Gap Achieved in Magnetic Infrared Nonlinear Optical Chalcogenide by Suppressing d-d Transitions**

Bin-Wen Liu,<sup>#</sup> Shao-Min Pei,<sup>#</sup> Xiao-Ming Jiang,<sup>\*</sup> and Guo-Cong Guo<sup>\*</sup>

#### Table of Contents

Experimental Procedures.....	1
Syntheses .....	1
Structural Refinement and Crystal Data .....	1
Infrared and UV–Vis–NIR Diffuse Reflectance Spectroscopy.....	2
Second-harmonic Generation Measurement .....	2
Laser-induced Damage Thershold Measurement.....	2
Electronic structures .....	2
Figures and Tables .....	3
References .....	6

## Experimental Procedures

### Syntheses

All starting reactants were handled inside an Ar-filled glovebox. A stoichiometric mixture of the La (99.9%, 1.16 mmol), Mn (99.99%, 0.48 mmol), Ga (99.99%, 1.43 mmol), S (99.99%, 3.35 mmol), and KCl (99.99%, 2.28 mmol) was loaded into a sealed silica tube to obtain  $[K_3Cl][Mn_2Ga_6S_{12}]$  (**1**). The tube was evacuated to  $10^{-4}$  Torr and placed into a furnace, heated to 300 °C in 6 h and kept at that temperature for 6 h, then heated and kept to 600 °C in 6 h, subsequently heated to 900 °C in 12h and maintained at 900 °C for 96 h, and finally slowly cooled down to 400 °C in 96 h. Several attempts without adding La as a reactant have been tried, and different synthesis conditions including variable temperatures, starting reactant types and molar ratios of starting reactants were used, however, all these attempts failed to synthesize the title phase. The La element may play the reaction promoter role in the formation of compound **1**. Energy-dispersive X-ray spectroscopy (EDS) analyses was performed with an EDS-equipped Hitachi S-3500 SEM spectrometer.

### Structural Refinement and Crystal Data

Single-crystal X-ray diffraction (XRD) dataset was collected on a Rigaku Pilatus CCD diffractometer equipped with a graphite-monochromated Mo-K $\alpha$  radiation ( $\lambda = 0.71073$  Å) at 293 K. The initial positions for all atoms were solved by direct methods, and the structures were refined by full-matrix least-squares techniques on  $F^2$  with anisotropic thermal parameters for all atoms. All the calculations were performed with the Siemens SHELXTL version 5 package of crystallographic software. Further details on the crystal structures investigation is on quoting the depository number CCDC-2100147. The powder XRD measurement was performed on a Rigaku MiniFlex II XRD.

### Infrared and UV-Vis-NIR Diffuse Reflectance Spectroscopy

Optical diffuse reflectance spectrum was collected at the room temperature using a Perkin-Elmer Lambda 900 UV-Vis-NIR spectrophotometer from 200 to 2500 nm. IR spectrum was recorded as solids in KBr matrices on a Nicolet Magana 750 FT-IR spectrophotometer (400-4000  $cm^{-1}$ ).

### Second-harmonic Generation (SHG) Measurement

The powder SHG measurements were performed by mean of a modified Kurtz-Perry method under a laser irradiation at 1910 nm. Microcrystalline **1** and AgGaS<sub>2</sub> (AGS) were sieved into several distinct particle size ranges (30–50, 50–75, 75–100, 100–150, and 150–200  $\mu m$ ) for the SHG measurements. The output of the fiber optic bundle was coupled to the entrance slit detected using a nitrogen-cooled CCD camera. The SHG signal intensities of **1** and AGS measured by modified Kurtz-Perry powder technique were evaluated by the angular average SHG susceptibility tensor square  $\langle d_{ijk}^2 \rangle$ :<sup>1</sup> Since compound **1** belongs to  $3m$  point group and three nonvanishing independent tensors left ( $d_{311}=d_{322}=d_{223}=d_{113}$ ,  $d_{211}=d_{112}=-d_{222}$ ,  $d_{333}$ ), effective SHG tensor  $d_{eff}$  can be simplified as:

$$\langle d^2 \rangle = \frac{19}{105}d_{333}^2 + \frac{26}{105}d_{333}d_{311} + \frac{38}{35}d_{113}^2 + \frac{10}{21}d_{222}^2$$

## Laser-induced Damage Thershold (LIDT) Measurement

The LIDTs measurement of microcrystalline sample (150 –200  $\mu\text{m}$ ) **1** and AGS were investigated by using a focused 1064 nm (pulse width  $\tau_p$  of 10 ns) laser beam. The measurements were performed by gradually increasing the laser power until the color of the sample changed, at which the laser power was defined as the damage threshold.

## Electronic structures

The electronic band structures, linear and NLO properties of compound **1** were performed using the ABINIT package based on density functional theory.<sup>23</sup> Generalized gradient approximation (GGA) parametrized by Perdew, Burke, and Ernzerhof (PBE) was chosen for the exchange-correlation functional. Projector-augmented plane-wave pseudopotentials with valence configurations K-3s<sup>2</sup>3p<sup>6</sup>4s<sup>1</sup>, Mn-3s<sup>2</sup>3p<sup>6</sup>4s<sup>2</sup>3d<sup>5</sup>, Ga-3d<sup>10</sup>4s<sup>2</sup>4p<sup>1</sup>, S-3s<sup>2</sup>3p<sup>4</sup>, and Cl-3s<sup>2</sup>3p<sup>5</sup> were selected with a plane-wave energy cut-off of 18 Hartree. The numerical integration of the Brillouin zone was performed using 5  $\times$  5  $\times$  2 Monkhorst–Pack  $\kappa$ -point meshes. Linear optical properties described by complex dielectric

function  $\epsilon_{ij, re} = \epsilon_{ij, re}(\omega) + \epsilon_{ij, im}(\omega)$  were calculated using 
$$\frac{4\pi}{\Omega} \sum_{nmk} f_{nm}(k) \frac{r_{nm}^i(k) r_{mn}^j(k)}{\omega_{mn}(k) - \omega} + \delta_{ij}$$
 where  $\epsilon_{re}(\omega)$  and  $\epsilon_{im}(\omega)$

are real and imaginary parts of the dielectric function, respectively,  $r_{nm}^i(k)$  is the position matrix elements between states n and m. The frequency-dependent SHG susceptibility tensors  $\chi_{ijk}(2\omega, \omega, \omega)$  were calculated using the density functional perturbation theory and “sum over states” method, where the SHG susceptibility is mainly contributed from three parts: the pure interband transition term  $\chi_{inter}(2\omega, \omega, \omega)$ , the intraband transition term  $\chi_{intra}(2\omega, \omega, \omega)$  describing the modulation of linear susceptibility by the intraband motion of electron, and the modulation term  $\chi_{mod}(2\omega, \omega, \omega)$  of intraband contribution by the interband motion-related polarization energy.[4] The orbital-resolved SHG susceptibility tensors were evaluated by multiplying each term in  $\chi_{inter}(2\omega, \omega, \omega)$ ,  $\chi_{intra}(2\omega, \omega, \omega)$  and  $\chi_{mod}(2\omega, \omega, \omega)$  by the normalized partial density of states of the involved orbitals, which fulfilled the restriction that the total contributions from all involved orbitals to each term are equal to 100%. The atomic-resolved SHG susceptibility tensors were obtained by the summation of contributions from all orbitals belonging to the target atom.

Figures and Tables

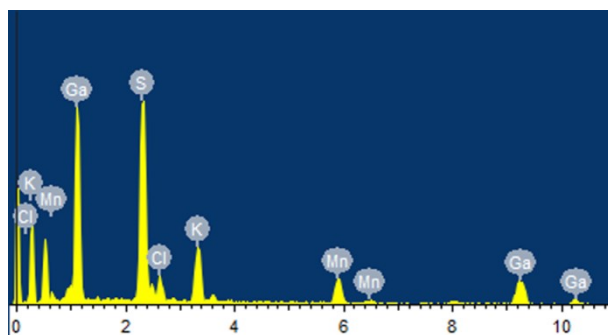


Fig. S1 The EDS results of 1.

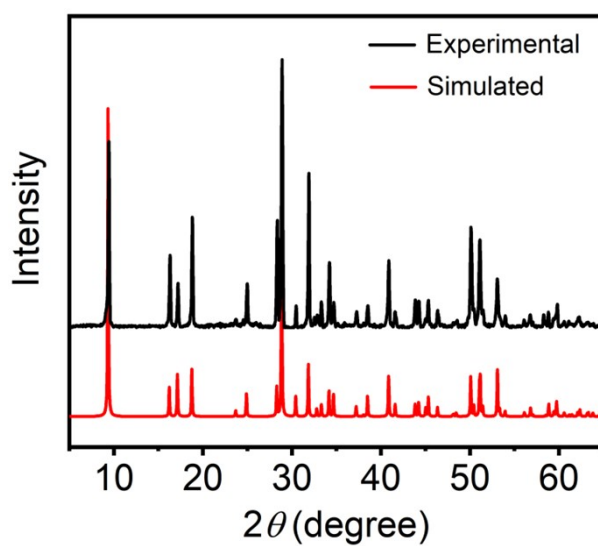
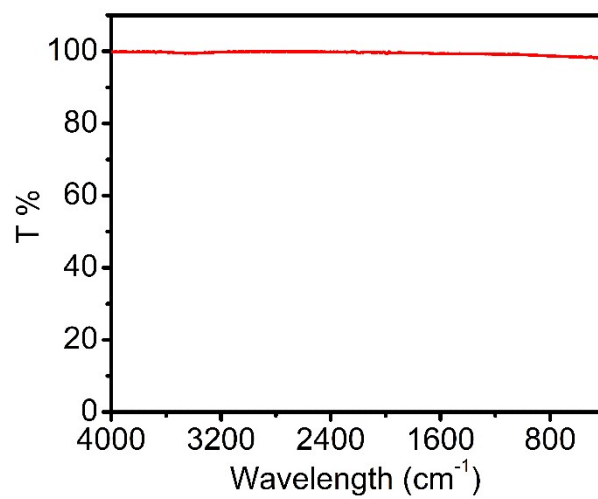
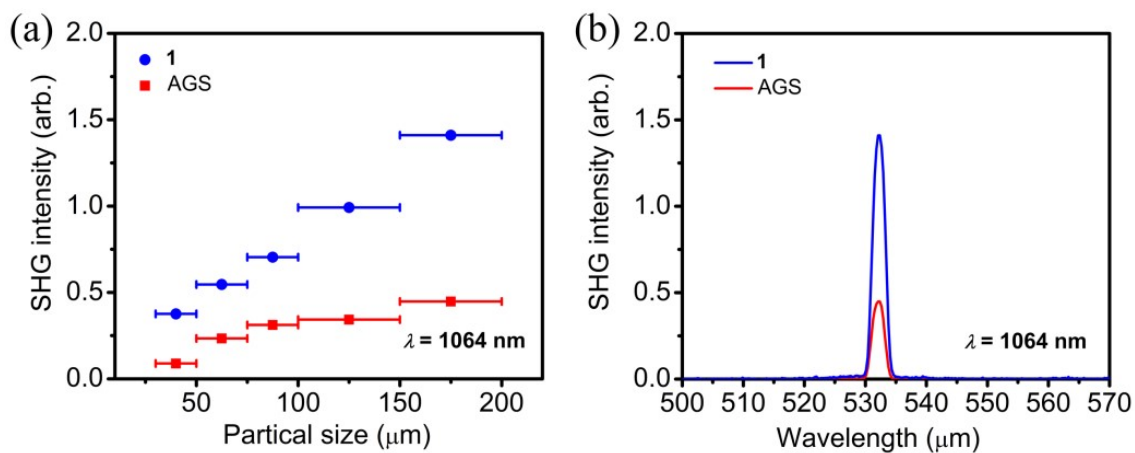


Fig. S2 The experimental and simulated XRD patterns of 1.



**Fig. S3** The IR spectra of **1**.



**Fig. S4** (a) Particle-size dependence of SHG intensities of **1** and AGS. (b) SHG intensities of **1** and AGS at particle sizes 150–200 nm under the radiation 1064 nm.

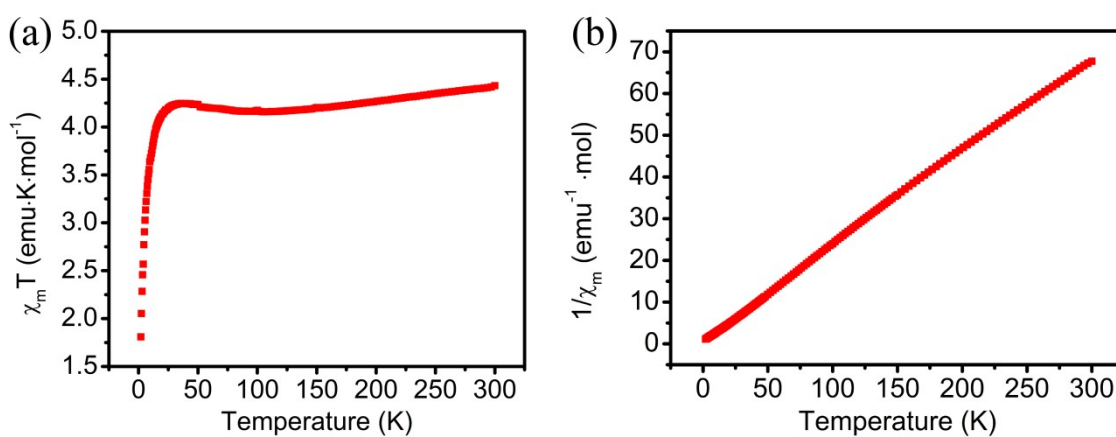


**Fig. S5** Variable-temperature  $\chi_m T$  (a) and  $1/\chi_m$  (b) curves of **1**.

**Table S1.** Crystallographic data and structure refinement parameters for **1**.

Empirical formula	[K <sub>3</sub> Cl][Mn <sub>2</sub> Ga <sub>6</sub> S <sub>12</sub> ]
<i>F</i> <sub>w</sub>	1065.67
Temperature (K)	293(2)
Space group	<i>P</i> 31 <i>c</i>
<i>a</i> (Å)	10.9208(4)
<i>c</i> (Å)	6.1774(3)
<i>V</i> (Å <sup>3</sup> )	638.04(6)
<i>Z</i>	1
<i>D</i> <sub>calcd</sub> (g·cm <sup>-3</sup> )	2.773
<i>μ</i> (mm <sup>-1</sup> )	8.754
<i>GOF</i> on <i>F</i> <sup>2</sup>	1.096
<i>R</i> <sub>1</sub> <sup><i>a</i></sup> ( <i>I</i> > 2σ( <i>I</i> ))	0.0358
<i>wR</i> <sub>2</sub> <sup><i>b</i></sup> ( <i>I</i> > 2σ( <i>I</i> ))	0.0960
<i>R</i> <sub>1</sub> <sup><i>a</i></sup> (all data)	0.0364
<i>wR</i> <sub>2</sub> <sup><i>b</i></sup> (all data)	0.0962
Δρ <sub>max</sub> /Δρ <sub>min</sub> , (e Å <sup>-3</sup> )	0.820/−0.523

$${}^a R = \sum ||F_o| - |F_c| | / \sum |F_o|, {}^b wR = (\sum (w(F_o^2 - F_c^2)^2) / \sum (w(F_o^2)^2))^{1/2}.$$

**Table S2.** Coordinates and equivalent isotropic displacement parameters of all crystallographically independent atoms in **1**.

Atoms	x	y	z	U(eq)
K1	0.2512(5)	0.0979(4)	0.175(4)	0.131(1)
Cl1	1.0000	1.0000	0.924(11)	0.19(3)
Mn1	0.6667	0.3333	0.9638(7)	0.0214(9)
Ga1	0.4216(1)	0.5326(2)	0.0465(1)	0.0167(4)
S1	0.5080(5)	0.3976(5)	0.1850(6)	0.0264(1)
S2	0.5538(5)	0.7532(4)	0.1895(7)	0.0202(8)

**Table S3.** Selected bond lengths [Å] for **1**.

Bond	Distance	Bond	Distance
K1–Cl1×6	2.85(4)	Ga1–S1	2.249(4)
Mn1–S1×3	2.565(5)	Ga1–S2	2.277(4)
Mn1–S2×3	2.699(5)	Ga1–S1	2.277(4)
		Ga1–S2	2.295(4)

**Table S4.** The laser-induced damage threshold of **1** and benchmark AgGaS<sub>2</sub>.

Compounds	Damage energy (mJ)	Spot area (cm <sup>2</sup> )	$\tau_p$ (ns)	Damage threshold [MW·cm <sup>-2</sup> ]
<b>1</b>	2.5	0.02496	10	100.0
AgGaS <sub>2</sub>	0.2	0.02496	10	8.0

**Table S5.** The average orbital-resolved contributions (%) of each atom type in **1** to the total SHG coefficient tensors ( $d_{21}$ ,  $d_{31}$  and  $d_{33}$ ) at the incident laser radiation of 1910 nm (0.65 eV). The 5th row is filled with average values of  $d_{21}$ ,  $d_{31}$  and  $d_{33}$ .

SHG(%)	S-s	S-p	Cl-s	Cl-p	K-s	K-p	Mn-s	Mn-p	Mn-d	Ga-s	Ga-p	Ga-d
$d_{21}$	4.5	30.4	0.04	23.9	0.7	0.4	0.5	0.7	3.1	30.4	4.5	0.9
$d_{31}$	5.7	32.7	1.1	13.1	0.5	3.2	6.0	0.7	1.8	31.4	3.1	0.9
$d_{33}$	5.1	32.5	1.2	11.3	0.7	2.1	1.7	1.8	4.7	34.6	4.0	0.2
Average	5.1	31.9	0.8	16.1	0.6	1.9	2.7	1.1	3.2	32.1	3.9	0.7

## References

1. S. K. Kurtz, T. T. Perry, *J. Appl. Phys.* 1968, **39**, 3798–3813.
2. X. Gonze, *Phys. Rev. A* 1995, **52**, 1086–1095.
3. P. Ghosez, X. Gonze, R. W. Godby, *Phys. Rev. B* 1997, **56**, 12811–12817.
4. S. Sharma, C. A. Draxl, *Phys. Scr.* 2004, **T109**, 128–134.